# High-temperature operating 894.6nm-VCSELs with extremely low threshold for Cs-based chip scale atomic clocks

**Jianwei Zhang,* Xing Zhang, Hongbo Zhu, Jian Zhang, Yongqiang Ning, Li Qin and Lijun Wang**

**State Key Laboratory of Luminescence and Application, Changchun Institute of Optics, Fine Mechanics and Physics, Chinese Academy of Sciences, 3888 Southeast Lake Road, Changchun, 130033, China*
*zjw1985@ciomp.ac.cn*

**Abstract:** We report on the design and fabrication of 894.6nm vertical-cavity surface-emitting lasers (VCSELs) with extremely low threshold at high temperatures, for use in chip-scale Cs atomic clocks. A new design method based on the analysis of the threshold gain and the desired carrier density for different active region structures was proposed to gain the low transparent current density. The increase of the threshold current at higher temperatures was successfully suppressed by introducing the large gain-cavity detuning of VCSEL. By detuning the gain-cavity mode to be −11nm, the minimum threshold current of only 0.23mA at 70 °C was achieved. The operating temperature for emitting the wavelength of 894.6nm was 110 °C, with the single mode suppression ratio (SMSR) of more than 25dB and the threshold current of only 0.32mA.



**OCIS codes:** (140.7260) Vertical cavity surface emitting lasers; (020.1670) Coherent optical effects; (160.3380) Laser materials; (270.3430) Laser theory.

## References and links

1. K. Iga, "Surface-emitting laser—its birth and generation of new optoelectronics field," IEEE J. Sel. Top. Quantum Electron. **6**(6), 1201–1215 (2000).
2. J. F. Seurin, C. L. Ghosh, V. Khalfin, A. Miglo, G. Xu, J. D. Wynn, P. Pradhan, and L. A. D. Asaro, "High-power vertical-cavity surface-emitting arrays," Proc. SPIE **6876**, 68760D (2008).
3. D. K. Serkland, G. M. Peake, K. M. Geib, R. Lutwak, R. M. Garvey, M. Varghese, and M. Mescher, "VCSELs for atomic clocks," Proc. SPIE **6132**, 613208 (2006).
4. Y. Zhang, S. Qu, and S. Gu, "Spin-polarized dark state free CPT state preparation with co-propagating left and right circularly polarized lasers," Opt. Express **20**(6), 6400–6405 (2012).
5. S. Knappe, V. Gerginov, P. D. D. Schwindt, V. Shah, H. G. Robinson, L. Hollberg, and J. Kitching, "Atomic vapor cells for chip-scale atomic clocks with improved long-term frequency stability," Opt. Lett. **30**(18), 2351–2353 (2005).
6. A. Al-Samaneh, M. Bou Sanayeh, M. J. Miah, W. Schwarz, D. Wahl, A. Kern, and R. Michalzik, "Polarization-stable vertical-cavity surface-emitting lasers with inverted grating relief for use in microscale atomic clocks," Appl. Phys. Lett. **101**(17), 171104 (2012).
7. D. W. Jenkins, "Optical constants of $Al_xGa_{1-x}As$," J. Appl. Phys. **68**(4), 1848–1853 (1990).
8. H. M. Tsai, S. Tang, S. Su, T. Chen, and C. Chiang, "Numerical simulation of temperature-dependence on distributed bragg reflector (DBR) and performance analyses for proton-implant/oxide confined VCSEL: comparison with transmission matrix, matrix calculating methods and macleod model," Proc. SPIE **6484**, 64840I (2007).
9. F. Bugge, G. Erbert, J. Fricke, S. Gramlich, R. Staske, H. Wenzel, U. Zeimer, and M. Weyers, "12 W continuous-wave diode lasers at 1120 nm with InGaAs quantum wells," Appl. Phys. Lett. **79**(13), 1965–1967 (2001).
10. S. L. Chuang, "Efficient band-structure calculations of strained quantum wells," Phys. Rev. B Condens. Matter **43**(12), 9649–9661 (1991).
11. S. B. Healy, E. P. O'Reilly, J. S. Gustavsson, P. Westbergh, Å. Haglund, A. Larsson, and A. Joel, "Active region design for high-speed 850-nm VCSELs," IEEE J. Sel. Top. Quantum Electron. **46**(4), 506–512 (2010).
12. Y. Zhang, Y. Ning, L. Zhang, J. Zhang, J. Zhang, Z. Wang, J. Zhang, Y. Zeng, and L. Wang, "Design and comparison of GaAs, GaAsP and InGaAlAs quantum-well active regions for 808-nm VCSELs," Opt. Express **19**(13), 12569–12581 (2011).
13. S. L. Chuang, *Physics of optoelectronic devices* (Wiley-Interscienc, 1995).

#237243 - $15.00 USD Received 2 Apr 2015; revised 19 May 2015; accepted 20 May 2015; published 27 May 2015

14. P. L. Derry, R. J. Fu, C. S. Hong, E. Y. Chan, and L. Figueroa, "Analysis of the high temperature characteristics of InGaAs- AlGaAs strained quantum-well Lasers," IEEE J. Quantum Electron. **28**(12), 2698–2705 (1992).
15. K. Iga, F. Koyama, and S. Kinoshita, "Surface emitting semiconductor lasers," IEEE J. Quantum Electron. **24**(9), 1845–1855 (1988).
16. S. Corzine, R. Geels, J. Scott, R. Yan, and L. Coldren, "Design of Fabry-Perot surace-emitting lasers with a periodic gain structure," IEEE J. Quantum Electron. **25**(6), 1513–1524 (1989).
17. J. Zhang, Y. Ning, Y. Zeng, J. Zhang, J. Zhang, X. Fu, C. Tong, and L. Wang, "Design and analysis of high-temperature operating 795 nm VCSELs for chip-scale atomic clocks," Laser Phys. Lett. **10**(4), 045802 (2013).
18. J. Wu, W. Xiao, and Y. M. Lu, "Temperature and wavelength dependence of gain and threshold current detuning with cavity resonance in vertical-cavity surface-emitting lasers," IET Optoelectron. **1**(5), 206–210 (2007).
19. I. A. Derebezov, V. A. Haisler, A. K. Bakarov, A. K. Kalagin, A. I. Toropov, M. M. Kachanova, T. A. Gavrilova, O. I. Semenova, D. B. Tretyakov, I. I. Beterov, V. M. Entin, and I. I. Ryabtsev, "Single-mode vertical-cavity surface emitting lasers for 87Rb-based chip-scale atomic clock," Semiconductors **44**(11), 1422–1426 (2010).

## 1. Introduction

VCSELs are the most miniature and economically efficient laser emitters developed so far. The unique geometry of VCSELs results in several significant advantages over their edge-emitting counterparts, including the low threshold current, circular output-beam profile, high modulation speed and small power consumption et al [1,2]. These advantages are presently attracting considerable attention for the applications in the CSAC (chip scale atomic clock) system [3,4]. The demonstration of CSAC using a modulated VCSEL paves the way to dramatically reduce the size and power consumption of atomic frequency standards. However, VCSELs used in those clocks must feature very critical requirements [5,6]. For example, VCSELs must be operated above the maximum ambient temperature at which the atomic sensor is specified to operate (>80°C for Cs CSAC). For low power consumption of the atomic clock, the power consumption of VCSEL should be limited to 2mW, which necessitates a threshold current below 1 mA. And VCSELs must emit a center wavelength of about 894.6 nm to employ the CPT effect of the cesium D1 line. But in fact, the threshold current of VCSELs usually increases quite rapidly with the elevated temperatures, due to the decreased optical gain received by the cavity mode. And the emission wavelength of VCSELs is also red shifted by the elevated temperature. These phenomena would greatly increase the power consumption of light sources and its control system in CSAC.

A new design of the VCSEL structure was proposed in this work, aiming at solving problems of VCSELs operating at high temperatures as the CSAC required. To decrease the threshold gain of VCSEL, the method of designing the InGaAs/AlGaAs multiple quantum wells (MQWs) was improved by considering the threshold gain of active region within VCSELs. The threshold current of VCSELs at high temperatures was kept consistent with that at RT by employing the concept of gain-cavity mode detuning. And it was also deduced that the minimum threshold current of VCSEL could occur at different temperatures where the cavity mode receives maximum optical gain by employing different gain-cavity detuning values. This was in contrast to typical VCSEL designs where the gain peak wavelength and the cavity resonance were nearly aligned at RT. At last, the VCSEL structure with −11nm gain-cavity detuning was fabricated, and the minimum threshold current of 0.23mA appeared at 70 °C for the device with 3.5μm-oxide aperture. To realize the emitting wavelength of 894.6nm as the CSAC required, the operating temperature was kept at 110 °C. The threshold current of VCSEL at this temperature was 0.32mA, which was consistent with that at RT. SMSR of VCSEL was more than 25dB from RT to the operating temperature.

## 2. 894.6 nm VCSEL description

A schematic view of the 894.6nm VCSEL structure was shown in Fig. 1. The top-emitting VCSEL structure was adopted to avoid the serious optical absorption of GaAs substrate at 894.6nm-wavelength [7]. The n-distributed bragg reflector (DBR) layers, the active region, and the p-DBR layers were sequentially grown on the n-GaAs substrate by metal-organic chemical vapor deposition (MOCVD). The enhancement of optical field in the active region was gained due to the cavity confinement, as shown in the inserted figure in Fig. 1.

#237243 - $15.00 USD Received 2 Apr 2015; revised 19 May 2015; accepted 20 May 2015; published 27 May 2015

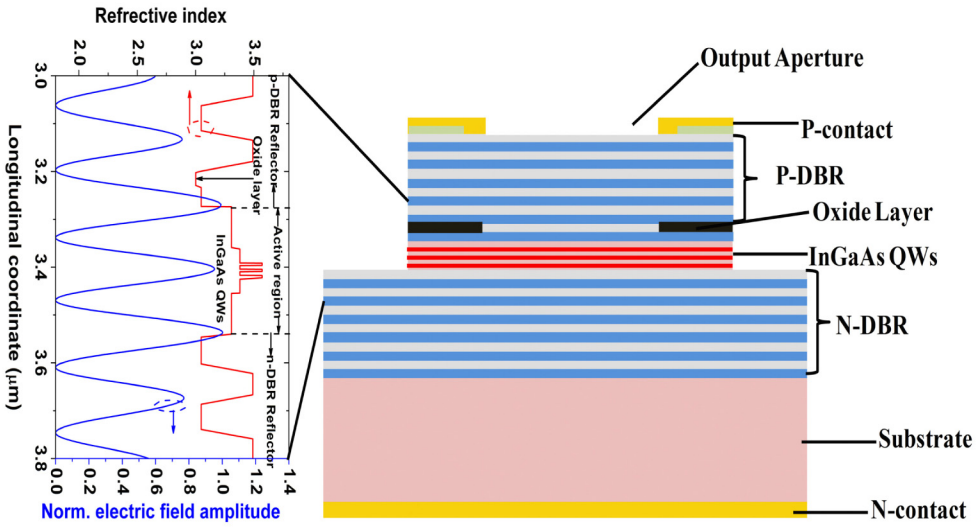


Fig. 1. Schematic cross section of the fabricated VCSEL structure, inserted was the normalized optical field distribution within the active region and the refractive index of each layer. The transmission matrix method (TMM) was utilized in the calculation.

The active region was composed of three compressively strained InGaAs quantum wells (QWs). And the position of QWs was configured just at the wave peak of optical field. The N-DBR and P-DBR consisted of 34.5 pairs and 22 pairs of $Al_{0.12}Ga_{0.88}As/Al_{0.9}Ga_{0.1}As$ layers, respectively. The interfaces within DBRs were graded in composition and doping concentration to minimize the free-carrier absorption and decrease the electrical resistance. For selective oxidation, a 30-nm-thick $Al_{0.98}Ga_{0.02}As$ layer was partially used instead of a high-Al-content layer in the p-DBR, near the active region.

## 3. Design of the low-threshold VCSEL structure

The emitting wavelength of VCSEL was determined by the cavity resonance. The temperature dependence of the cavity resonance was calculated by the TMM, and the value of 0.06nm/°C was corresponded with the reported results of AlGaAs based VCSEL structures [8]. To realize the emitting wavelength of 894.6nm at 85°C, which was the Cs-vapor cell temperature of our CSAC system, the cavity resonance wavelength at RT was set to be 891nm.

InGaAs/AlGaAs strain quantum wells (QW) had been widely employed for lasers emitting at wavelengths of near-infrared and demonstrated superior gain characteristics [9]. Therefore, we chose three InGaAs QWs separated by $Al_{0.3}Ga_{0.7}As$ barriers to form the active region. For optimization purposes of the active region, QWs with different compositions and thicknesses were designed, aiming at changing the alignment amount between the cavity resonance and the gain peak wavelength at RT. Three types of active regions with gain peak wavelength of 870nm, 880nm, 890nm were designed, and the corresponding gain-cavity detuning was −21nm, −11nm, −1nm, respectively. The threshold current–temperature characteristic of VCSELs in relation to the gain-cavity detuning at room temperature (RT) would be presented and evaluated later.

To analyze the threshold gain and the gain-cavity mode characteristics of VCSELs, the gain calculation was carried out to obtain the gain characteristics of active region, which was consisted of three QWs separated by $Al_{0.3}Ga_{0.7}As$ barriers. As the gain calculations were for the QW group within the active region, the $k \cdot p$ theory with valence band mixing effects was employed to calculate quantum well subbands [10–12]. In the case of valence mixing, the theories of parabolic band approximation were not feasible. Based on the developed theories in Ref [13,14], the gain spectrum could be expressed in the numerical integration over $k_t$:

#237243 - $15.00 USD Received 2 Apr 2015; revised 19 May 2015; accepted 20 May 2015; published 27 May 2015

$$g(E) = \frac{g_0}{2\pi tE}\sum_{i,j}\int_0^{\infty}\frac{(\pi/\Gamma)f_{dip}(k_t)M_b(f_j - f_i)dk_t^2}{1+(E_{cj}(k_t) - E_{kpi}(k_t) - E^2)/\Gamma} \quad (1)$$

Where $t$ is the quantum well thickness, and $\Gamma = h/\tau_{scat}$ is the broadening due to intraband scattering relaxation time $\tau_{scat}$. $E_{cj}$ and $E_{kpi}$ are the jth conduction subband and the ith valence subband from the $k{\cdot}p$ calculation. $M_b$ is the bulk dipole momentum. $f_j$ and $f_i$ are the Fermi functions. The sum is over all possible valence and conduction subbands, and $g_0$ is a constant defined as

$$g_0 = \frac{\pi q^2 h}{\varepsilon_0 c m_0^2 n}. \quad (2)$$

Where q is free electron charge; $n$ is the real part of the refractive index, and all other symbols have their usual meanings.

Figure 2 showed the calculated indium content and the corresponding thickness of InGaAs QWs for different gain peak wavelengths of active region. It was shown that both the indium content and the thickness of QW should be adjusted to maintain the gain peak wavelength. In order to keep the gain peak wavelength unchanged, the indium content must be decreased with increasing QW thickness. For the fixed indium content, increasing the thickness of QW could red shift the gain peak wavelength, due to the reduced energy band splitting of QWs [10]. The gain peak wavelength was also red shifted when the indium content was increased for the fixed thickness of QW. But this was mainly caused by the increased energy band wavelength when the indium content of InGaAs bulk material was increased.

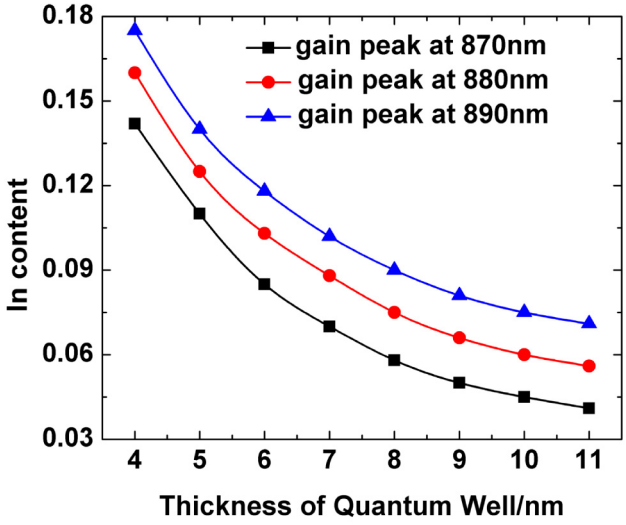


Fig. 2. Calculated relationships between indium contents and thicknesses of InGaAs QWs, which provided the gain peak wavelengths of 870nm, 880nm and 890nm at RT, with the fixed barriers of $Al_{0.3}Ga_{0.7}As$.

Although the gain peak wavelength of active region could be realized by various indium contents and thicknesses of InGaAs QWs, their gain characteristics were different and needed to be optimized to realize the low threshold gain of VCSELs. The threshold gain of VCSELs was the minimum optical gain needed for lasing, which was used to overcome the total optical loss, including diffraction loss, absorption and scattering losses of the laser cavity as well as light output from the surface. The threshold gain could be expressed as follows [15]

#237243 - $15.00 USD Received 2 Apr 2015; revised 19 May 2015; accepted 20 May 2015; published 27 May 2015

$$g_{th} = \alpha_a + \frac{1}{\Gamma_r d_a}\left[\alpha_i (L - d_a) + \ln\frac{1}{\sqrt{R_t R_b}}\right]. \quad (3)$$

Where $\alpha_i$ and $\alpha_a$ are internal losses in the passive and active sections. $R_t$ and $R_b$ are the reflectivity of the front and back DBR reflectors, determined by the TMM. $L$ and $d_a$ are the thickness of inner cavity and active region, respectively. The relative confinement factor $\Gamma_r$ is defined by [16]

$$\Gamma_r = \frac{L}{d_a}\frac{\int_{d_a} |E(z)|^2 \, dz}{\int_L |E(z)|^2 \, dz}. \quad (4)$$

Where $E$ is the spatially distribution of electric field within VCSELs. The distribution of electric field is calculated by the TMM.

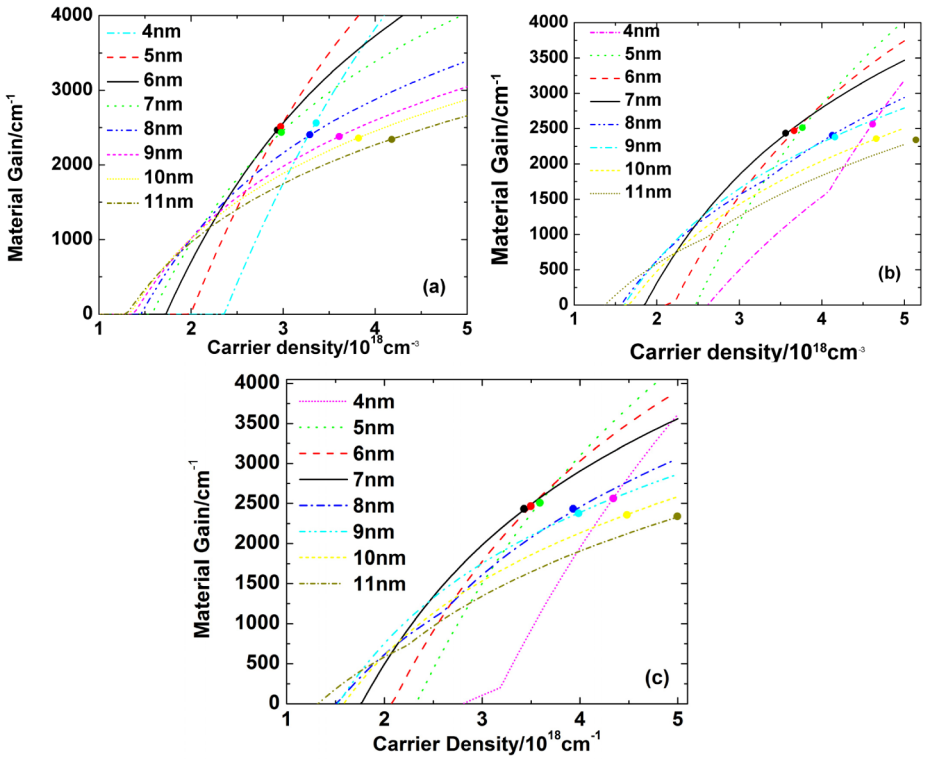


Fig. 3. The peak material gain of InGaAs QWs providing the gain peak wavelength of (a) 870nm, (b) 880nm and (c) 890nm as a function of carrier density at RT. The QW thickness varied from 4nm to 11nm. The threshold gain of VCSELs composed by these QWs was respectively indicated on the lines by the solid circle.

Figure 3 depicted the gain characteristics of InGaAs QWs providing the gain peak wavelength of 870nm, 880nm and 890nm as a function of carrier density at RT. The threshold gain of VCSELs composed by these QWs was also indicated on the lines by the solid circle, respectively. The saturation of material gain was observed as the first quantized level of QW saturated. And a sharp increase of material gain for the 4nm-QW curves in Figs. 3(b) and 3(c) was caused by the domination of the second quantized level.

The decrease of differential gain *dg/dn* (slopes of the curves) was observed in Fig. 3(a)-3(c) when the QW thickness increased from 5nm to 11nm. This was attributed to the decreased curvature of the first valence band, which resulted in higher densities of valence

#237243 - $15.00 USD Received 2 Apr 2015; revised 19 May 2015; accepted 20 May 2015; published 27 May 2015

states [17]. Except for this, the thicker QW also allowed more valence-band levels. The inflection point on the 11nm-QW curve in Figs. 3(b) and 3(c) suggested the onset of other higher quantized energy states.

The slightly reduced threshold gain was observed in Fig. 3(a)-3(c) when the QW thickness increased from 4nm to 11nm. And this was caused by the increased optical confinement factor. However, the carrier density needed to reach the threshold gain was higher for the thicker QW when the thickness was more than 7nm, and vice versa. Although the active region consisted of 7nm-thickess QW showed the minimum carrier density to reach the threshold gain, the differential gain and saturation value of the gain curve were not high enough. To sum up, the finally optimized InGaAs QW thickness was 5 nm for all the three types of active regions with different gain peak wavelengths.

The lasing wavelength of VCSELs was determined by the resonance frequency in the cavity, which was called the cavity mode. Thus the optical gain on the gain spectra of QWs received by the cavity mode was effective for VCSELs [18]. And this gain value was simplified as cavity-mode gain in the following discussions. Since the required threshold gain in Eq. (3) of VCSEL was nearly constant, the higher cavity-mode gain required lower carrier density to maintain the threshold condition. Thus, to efficiently reduce the threshold current, the high cavity-mode gain at the operating temperature was preferred in designing the VCSEL structure.

#237243 - $15.00 USD Received 2 Apr 2015; revised 19 May 2015; accepted 20 May 2015; published 27 May 2015

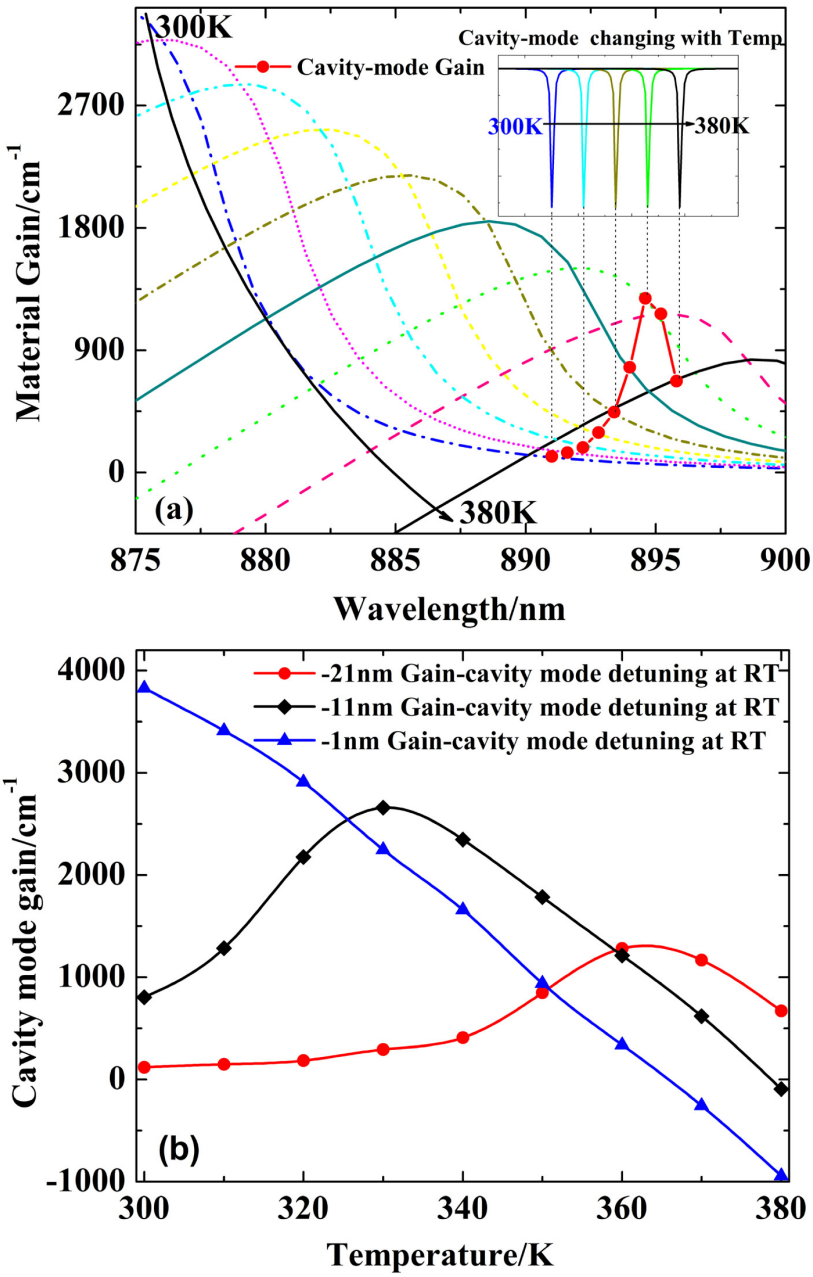


Fig. 4. (a) Gain spectra of active region with the gain peak wavelength of 870nm at RT for different temperatures. Inserted figure was the change of cavity mode with temperature. The red solid circle indicated the cavity-mode gain at different temperatures, which was the overlap of gain spectra and cavity mode. (b) Temperature dependence of the cavity-mode gain for different gain-cavity mode detuning values of −21nm, −11nm, −1nm at RT.

Figure 4 (a) illustrated the gain spectra-temperature characteristics of VCSELs with the gain-cavity detuning of −21nm at RT. The carrier density for the gain spectra calculation was $3.5 \times 10^{18}\text{cm}^{-3}$. The gain value received by the cavity mode at different temperatures was also indicated by the red solid circle. The cavity mode at RT was 891nm, and the temperature

#237243 - $15.00 USD Received 2 Apr 2015; revised 19 May 2015; accepted 20 May 2015; published 27 May 2015

dependence of the cavity resonance was 0.06nm/°C. The rapid decrease of peak gain with the elevated temperature was observed, and the temperature dependence of gain-peak wavelength was 0.3nm/°C. Thus for VCSELs with negative gain-cavity detuning, the gain peak wavelength approached to the cavity mode as the temperature increasing, and then exceeded the cavity mode at higher temperatures. As a result, the corresponding cavity-mode gain increased with the elevated temperature firstly, but then decreased when the gain-cavity mode offset became positive, shown as the red circle line in Fig. 4 (a).

The cavity-mode gain of three VCSELs with different gain-cavity detuning but identical cavity mode of 891nm at RT was illustrated as a function of temperature in Fig. 4 (b). It exhibits a maximum cavity-mode gain at around 300K when the gain-cavity detuning was −1nm. By enlarging the gain-cavity mode detuning to be −11nm and −21nm, the point of maximum cavity mode gain was shifted toward higher temperatures of 330k and 363k. The latter had a maximum cavity-mode gain near the operating temperature of the atomic clocks (85°C). However, the former structure could also provide almost the same cavity-mode gain at this temperature. Except for this, the cavity-mode gain of the former structure at the operating temperature was consistent with that at RT. As a result, the parameters of VCSELs related to the cavity-mode gain could be characterized and validated at RT. Therefore, the VCSEL structure with −11nm gain-cavity detuning had been employed in the VCSELs reported later. As the threshold current was in inverse proportion to the cavity mode gain, the minimum threshold current would occur at higher temperatures where the cavity mode received maximum optical gain. The minimum threshold current of designed VCSEL would appear at about 330K, corresponding to the maximum point of the black diamond line in Fig. 4 (b).

## 4. Results and discussions

The VCSEL with −11nm gain-cavity detuning had been fabricated and characterized. Figure 5 depicted the measured CW light–current (P–I) characteristics of VCSELs with 3.5μm active diameter at different temperatures. A characteristic feature was the reduction of the threshold current as a result of the increasing cavity-mode gain when the temperature increased from 22°C to 70°C, as shown in the inserted figure. And then the threshold current increased as the temperature continued to increase. The dependence of the threshold current to temperature was consistent with that of the cavity-mode gain in Fig. 4 (b). The change of slope efficiency dP/dI with temperature was contrary to that of threshold current, due to its positive proportion to the cavity-mode gain.

#237243 - $15.00 USD Received 2 Apr 2015; revised 19 May 2015; accepted 20 May 2015; published 27 May 2015

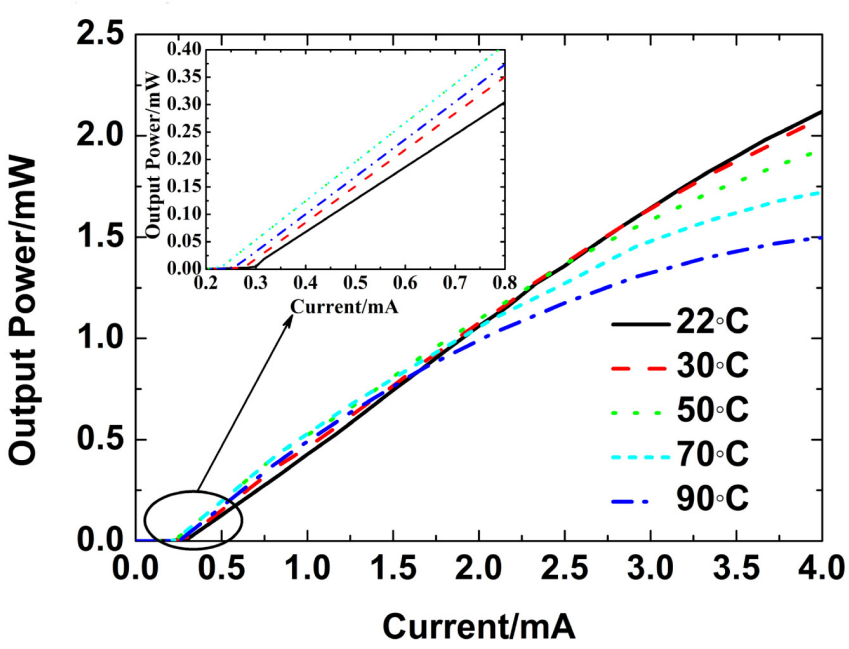


Fig. 5. CW operation characteristics of a standard VCSEL with 3.5 μm active diameter at different substrate temperatures. The P-I characteristic near the threshold current was enlarged in the inserted figure.

Figure 6 showed the measured CW threshold current and output wavelength–temperature characteristics. Inserted were the optical spectrum at I = 1mA for the substrate temperature of RT and 110°C, respectively. As was typical of the gain-cavity detuning VCSELs, we found a distinct minimum in the threshold current at a particular substrate temperature of 70°C. And the threshold current at this point was only 0.23mA. For this point, further raising or decreasing the temperature would serve to increase the separation between the cavity mode and the gain peak, resulting in a rapidly increased threshold current. And this was consistent with the above theoretical analysis results related to the dependence of cavity-mode gain on temperature in Fig. 4 (b).

#237243 - $15.00 USD Received 2 Apr 2015; revised 19 May 2015; accepted 20 May 2015; published 27 May 2015

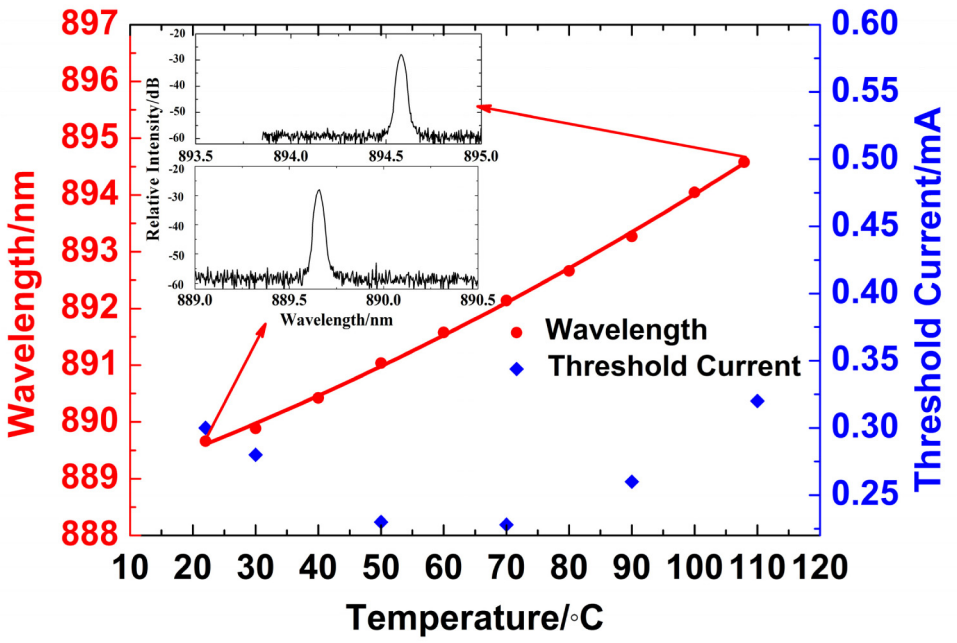


Fig. 6. Threshold current and optical output wavelength under the operating current of I = 1mA versus substrate temperature. Inserted were the optical spectrum at RT and operating temperatures.

The increased red-shift rate of emitting wavelength with temperature was observed in Fig. 6. And this was caused by the degradation of carrier confinement within QWs, due to the accelerated accumulation of internal self-heating at higher temperatures. The emitting wavelength of VCSEL was 889.6nm at RT, which was about 1.4nm shorter than the original cavity mode of 891nm. And the small oxide aperture size might be the main reason. As the oxide aperture size was reduced to be less than 4μm, the reduction of the mode volume could lead to the rapid shift of the resonant wavelength toward the short-wavelength [19]. For the 894.6nm-emitting, the operating temperature of VCSEL was improved to 110°C, much higher than the CSAC required. However, the threshold current at such high temperature was only 0.32mA, and it was slightly higher than the threshold current of 0.31mA at RT. The inserted optical spectrum showed single mode operation with an SMSR of more than 25 dB from RT to the operating temperature of 110°C.

## 5. Conclusions

In summary, 894.6-nm VCSELs was designed and fabricated to optimize its performance at high temperatures, for use in Chip-Scale Cs atomic clocks. The QWs with variant compositions and thicknesses were theoretically optimized, promising both high material gain and differential gain. The temperature sensitivity of the cavity-mode gain was analyzed for VCSEL structures with identical cavity mode but different gain-cavity detuning over a broad temperature range (300–380 K). It was found that the cavity-mode gain had a minimum at a temperature that was related to the gain-cavity offset at RT. The VCSEL structure with −11nm gain-cavity detuning was fabricated and characterized. Such a detuning value promised extremely low threshold currents at the operating temperature from RT to the operating temperature of 110°C.

#237243 - $15.00 USD Received 2 Apr 2015; revised 19 May 2015; accepted 20 May 2015; published 27 May 2015

**Acknowledgments**

This work is supported by the National Natural Science Foundation of China under Grant Nos. 11404326, 61234004, 51172225, and 61176045, the Foundation of Jilin Province under Grant No. 20140520113JH.

#237243 - $15.00 USD Received 2 Apr 2015; revised 19 May 2015; accepted 20 May 2015; published 27 May 2015